Performance Analysis of Grid Forming Converters for a Didactic Smart Grid System

Macit Tozak
Department of Electrical and Electronics Engineering
Manisa Celal Bayar University
Manisa, Turkey
email: macit.tozak@cbu.edu.tr

Sezai Taskin
Department of Electrical and Electronics Engineering
Manisa Celal Bayar University
Manisa, Turkey
email: sezai.taskin@cbu.edu.tr

Ibrahim Sengor
MaREI Centre, ERI and the School of Engineering
University College Cork
Cork, Ireland
and Department of Electrical and Electronics Engineering
Izmir Katip Celebi University
İzmir, Turkey
email: isengor@ucc.ie

2022 57th International Universities Power Engineering Conference (UPEC) | 978-1-6654-5505-3/22/$31.00 ©2022 IEEE | DOI: 10.1109/UPEC55022.2022.9917939

***Abstract*— Grid forming control for inverter-dominated power systems of the future is crucial as it enables more renewable penetration and provides enhanced stability. In this paper, a power system that consists of both Synchronous Machines (SM) and Grid Forming Controlled PV system is modeled and simulated in MATLAB®/ Simulink®. Moreover, the real parameters of laboratory pieces of equipment in Manisa Celal Bayar University Smart Grid Laboratory (MCBU-SGLab) are used throughout the study. In addition, various Grid Forming Converter control methods such as droop control, matching control, and dispatchable virtual oscillator control are compared in terms of frequency stability under different conditions.**

Keywords*— *grid forming control, grid forming converters, grid following converters, low inertia systems, inverter interfaced systems, converter-based resources

I. INTRODUCTION

Renewable-based generation units' demand which are Inverter Based Resources (IBR) is increasing gradually in order to prevent the climate change, the effect of which is being felt more and more in the world, to replace the decreasing fossil fuels, and to provide cost-effective. However, it is worth underlining that IBRs lead to a reduction in the total inertia of the system [1]. This adversely affects the frequency response of the system, making it very difficult to control the frequency and maintain the supply-demand balance [2]. Besides their negative effects, power converters have a superior feature and can respond within 1-30s [3]. This is a very short time scale that even includes the SM's inertial response. So, proper control techniques have gained importance to effectively use this potential. Furthermore, IBRs are controlled as Grid Following (GFL) and Grid Forming (GFM) modes of operations [4]. Although almost all of the current IBRs are installed in GFL mode, it is not satisfying in terms of stability issues in the converter-dominated system. As an alternative solution, GFM control has been taking the attention of both academia and industry in recent years because of being a critical asset for future power grids [5]. It originated from the need for a source that forms voltage and frequency in isolated microgrids and then it was adapted to large-scale power grids and HVDC systems [6]. It is necessary to use GFM converters for power systems with IBR penetration levels above 75-80% to maintain system stability [7]. While the IBR penetration is increasing day by day in power systems, GFM converters are still under development and any satisfactory solution that meets expectations has not been found [6].They are expected to include some specifications such as black start capability, load sharing and drooping, frequency and voltage regulation [8]. Also, it is required to behave like a voltage source in normal operation conditions and to work autonomously when it is isolated from bulk generation [9].

GFM control techniques were discussed from various aspects in the literature. The response of a power system with GFM converters and SMs to a sudden load change was evaluated in [8]. Also, the interaction of IBRs controlled by different GFM methods with SMs was tested on the IEEE 9 bus system. In [10], three-phase, electromechanical models for both GFMs and GFLs were developed. They performed the dynamic simulation of the distribution system by integrating these models into a three-phase distribution grid model with a high penetration level of IBRs. In [11], a decentralized secondary frequency controller for an isolated microgrid, which does not require a communication infrastructure, was presented with the optimal LQR method. The authors in [12] designed an autonomous, dual active power-frequency droop control scheme that can change the PV system's droop characteristic to control the PV system's active power and contribute to both slow and fast frequency response. Liu et al. [13] proposed the unified modeling method to analyze the dynamic performance of Virtual Synchronous Generator-based IBRs that vary in different operating modes. Singhal et al. [14] demonstrated that it is possible to fully coordinate GFM and GFL inverters for accurate power sharing, frequency/voltage regulation, and circulating reactive power reduction in microgrids without the support of any SMs or large power systems. In [15], a generalized control architecture for GFM converters was proposed from the perspective of multivariable feedback control, and various GFM control methods and their derivatives were combined in a multivariable feedback control transfer matrix. As a continuation of previous work, in [16], a generalized multivariate GFM structure was developed for cascaded controlled power converters.

This paper introduces the effect of the GFM converter on the didactic smart grid system in MCBU-SGLab. MCBU-SGLab includes two SMs, a thermal power plant emulator that represents a slack bus, a solar power plant emulator, transformers, and two different length transmission lines. The simulation techniques suggested for GFM control methods in [17] were adapted to our test system and it was observed that the system works stably even under large disturbances. So the frequency response and active power injections are tested on the didactic system under large disturbance for different GFM control techniques such as droop control, matching control,

The work of I. Sengor was supported by Science Foundation Ireland (SFI) under grant no. 12/RC/2302_P2.

and dispatchable virtual oscillator control (dVOC) in MATLAB®/Simulink®.

II. Comparison of GFL and GFM Converters

GFM and GFL techniques are used to control IBRs.The basic difference between GFL and GFM modes depends on their interaction with the grid. Synchronization of GFM converters is based on power balance like Synchronous Generators (SG) rather than Phase Locked Loop (PLL) measurement as in GFL converter [18]. So, it is not required to follow the voltage phasor of the Point of Common Coupling (PCC) as long as it does not exceed the allowed current limitations. GFL converters have poor stability characteristics in weak grids although additional improvements have been provided by some methods such as current controlled droop and virtual synchronous generation control, and they cannot operate in standalone mode [19]. GFL and GFM converters are compared in Table I.

Control structures of GFL and GFM converters are given in Fig. 1 and Fig. 2, respectively. In these figures, C_p denotes the power control loop and C_v is the voltage control loop.

III. Grid Forming Control Methods

In literature, there are many GFM control methods. However, only 3 of them are described because they are used for testing purposes, which are droop control, matching control, and dVOC.

A. Droop Control

Droop control was first proposed by [20]. It emulates the speed droop property of SM. Droop control is often followed by a low pass filter to eliminate the measurement noise. Frequency dynamics of droop control are given in (1) and (2).

$$\dot{\theta} = \omega \tag{1}$$

$$\omega = \omega^{ref} + d_\omega (P^{ref} - P) \tag{2}$$

In (1) and (2), ω is the measured frequency P is the measured active power at PCC. ω^{ref} and P^{ref} are the reference frequency and active power, respectively. d_ω is the droop coefficient.

TABLE I. Comparison of GFL and GFM Converters

Property	GFL	GFM
Primary objective	Active power injection	Grid supporting
Modeling	Current source followed by high parallel impedance	Voltage source followed by low series impedance
Synchronization	By PLL. The voltage phasor at PCC is tightly followed by the converter.	By power balance. Once the converter is synchronized, it is not needed to follow v_{PCC}, similar to SG.
Standalone (islanded) mode	No	Possible
Reaction	Slower	Faster
Black start capability	No	Possible

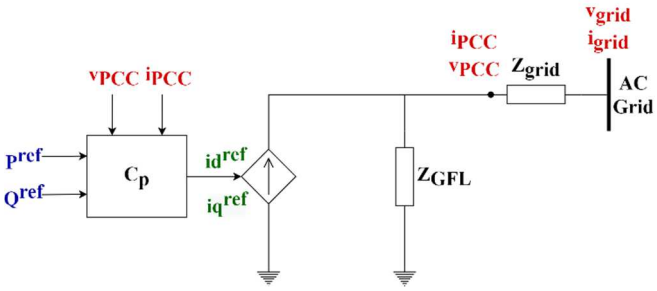

Fig. 1. Control structure of GFL converter

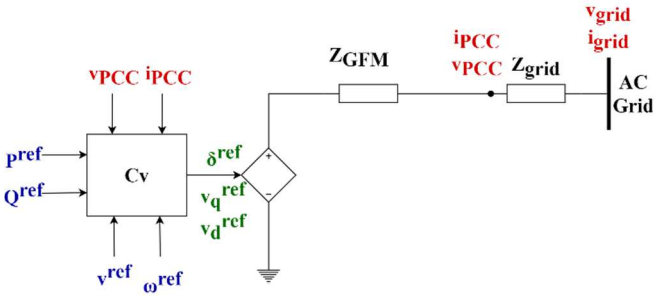

Fig. 2. Control structure of GFM converter

Output voltage error between reference and measured voltages is overcome by the PI controller in (3). Here v_d^{ref} is d axis reference voltage, k_p is proportional, and k_i is integral gain constants of PI controller.

$$v_d^{ref} = k_p\left(v^{ref} - \|v_{PCC,dq}\|\right) + k_i \int_0^t \left(v^{ref} - \|v_{PCC,dq}(\tau)\|\right) d\tau \tag{3}$$

B. Matching Control

Matching control is based on the similarities between converter dynamics and SM dynamics. Frequency change in SM represents power imbalance. Similarly, the change in DC link voltage in converters indicates power imbalance. From this point of view, it is thought that the DC input current of the converters can be used to control the AC output power, similar to the SM input torque. Matching control is based on such similarities between SMs and converters [21].

Matching control provides knowledge of the DC dynamics of the converter and whether source limits are exceeded or not because it considers the DC measurements, too. Matching control angle dynamics are given as follows:

$$\dot{\theta} = k_\theta v_{dc} \tag{4}$$

$$k_\theta = \frac{\omega^{ref}}{v^{ref}{}_{dc}} \tag{5}$$

In (4) and (5), k_θ refers to ratio of reference frequency to DC bus voltage ($v^{ref}{}_{dc}$).

AC output voltage in (7) is controlled according to modulation index μ given in (6).

$$\mu = k_p\left(v^{ref} - \|v_{PCC,dq}\|\right) + k_i \int_0^t \left(v^{ref} - \|v_{PCC,dq}(\tau)\|\right) d\tau \tag{6}$$

$$v_{PCC,\alpha\beta}{}^{ref} = \mu[-\sin\theta \ \cos\theta]^T \quad (7)$$

C. Dispatchable Virtual Oscillator Control

dVOC is a decentralized control strategy that requires only local measurements with adjustable droop characteristics. It guarantees almost global asymptotic stability of massively interconnected converters [22]. The frequency and voltage dynamics of dVOC are given in (8) and (9) where η and α refer to the positive gain constant.

$$\dot{\theta} = \omega^{ref} + \eta\left(\frac{P^{ref}}{(v^{ref})^2} - \frac{P}{\left\|v_{PCC,dq}\right\|^2}\right) \quad (8)$$

$$\begin{aligned}&\left\|\dot{v}_{PCC,dq}{}^{ref}\right\| \\ &= \eta\left(\frac{Q^{ref}}{(v^{ref})^2} - \frac{Q}{\left\|v_{PCC,dq}{}^{ref}\right\|^2}\right)\left\|v_{PCC,dq}{}^{ref}\right\| \\ &+ \frac{\eta\alpha}{(v^{ref})^2}\left((v^{ref})^2 \right. \\ &\left. - \left\|v_{PCC,dq}{}^{ref}\right\|^2\right)\left\|v_{PCC,dq}{}^{ref}\right\|\end{aligned} \quad (9)$$

IV. System Model and Simulation Results

The smart grid didactic system in MCBU-SGlab is modeled in MATLAB®/Simulink® to analyze the effects of GFM control methods. In the system, Hydro Power Plant (HPP) and Wind Power Plant (WPP) are represented by synchronous machines, Thermal Power Plant (TPP) which means the infinite bus is represented by a 3 phase power supply, and Solar Power Plant (SPP) is represented by a PV panel which is connected to the grid via GFM converter. Also, two transmission lines and transformers are used. The single-line diagram of the test system is given in Fig. 3. System parameters are given in Table II.

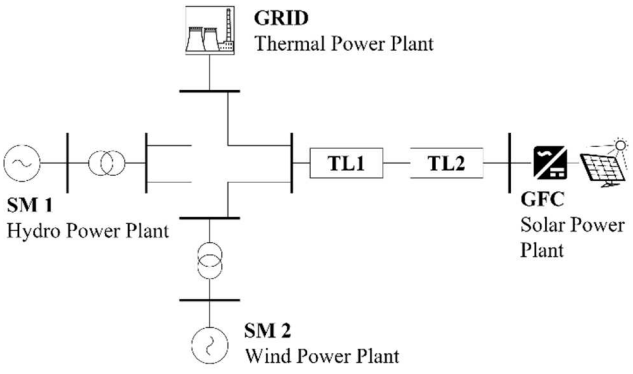

Fig. 3. Single line diagram of the test system.

The smart grid system in MCBU-SGlab is modeled in Matlab/ SIMULINK. Each source is set to supply the 0.75 p.u active power. Then, 3 GFM control methods are tested under normal operating conditions and 0.75 p.u large disturbance at 15 s. Fig. 4, Fig. 5, and Fig. 6 show the frequencies of each bus of the system at which there is a GFM converter controlled by droop control, matching control and dVOC, respectively. Also, for all cases, the frequency at the bus to which the GFM converter is connected is compared in Fig. 7. The frequency response of converters at initialization is get as follows. Among converters, the one controlled by dVOC method is settled the fastest in 1.5601 s, as the slowest one is droop control in 4.7771 s. The maximum overshoot is observed in matching control as 5.71%, while the minimum one is observed in dVOC as 0.07%. The frequency response at large disturbance at 15 s, matching controlled converter settled the fastest in 1.1545 s, while dVOC controlled one is the slowest in 1.1905 s. After disturbance, the maximum deviation is obtained in matching controlled converter response as 0.3748%, while the minimum one is get in droop control as 0.3510%. Frequency response quantities for all control methods are given in Table III.

The active power injections at each bus of the system at which there is the GFM converter controlled by droop control, matching control, and dVOC are shown in Fig. 8, Fig. 9, and Fig. 10, respectively. Besides, the active power injections at the bus to which the GFM converter is connected is compared in Fig. 11 for all control methods. The active power response at GFM-controlled converters is obtained as follows. The converter controlled with the dVOC method is settled the fastest in 1.8441 s, while the droop-controlled one is settled the slowest in 6.7592 s at initialization. The maximum overshoot is observed as 317.09% in the dVOC, while the minimum is in the matching control as 28.33% at initialization. After the disturbance, the minimum settling time is observed in matching control in 1.7446 s and the maximum overshoot is obtained as 59.39% in dVOC. Active power response quantities for all control methods are given in Table IV.

As a result, while the response against disturbance of these three control methods in the test system is almost the same, there are noticeable differences in initial responses for both frequency and active power. In frequency response, while the initial peak of the matching control draws attention, the dVOC shows the smallest overshoot. Moreover, the frequency of the dVOC can be stabilized the fastest with the lowest initial peak. However, the initial active power peak at the dVOC is very high compared to others. During high disturbance at 15 s, both frequency and active power response of all control methods are almost the same.

TABLE II. System Parameters

Part of the System	Parameter	Value
Grid	Base power (S_b)	0.8 KVA
	Base voltage (V_b)	400 V
	Frequency	50 Hz.
Synchronous machine	Rated power	0.8 KVA
	Inertia constant (H)	3.7 s
	Generator time constant (τ_g)	0.2 s
	Droop percentage (D_p)	2%
Converter	Filter inductance (L_f)	10 mH
	Filter capacitance (C_f)	600 uF
	Converter time constant (τ_c)	0.05 s
Transformer	Rated power	0.8 KVA
Transmission line 1	Resistance (RTL1)	12 Ohm
	Inductance (LTL1)	290 mH
Transmission Line 2	Resistance (RTL2)	3.3 Ohm
	Inductance (LTL2)	80 mH

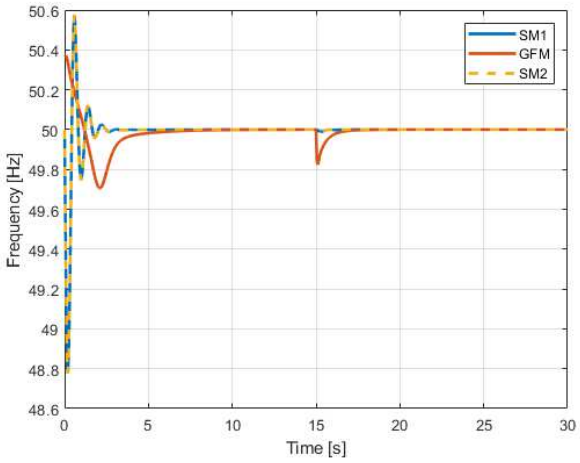

Fig. 4. Frequency of the system consists of 2 SM and a GFM with droop control

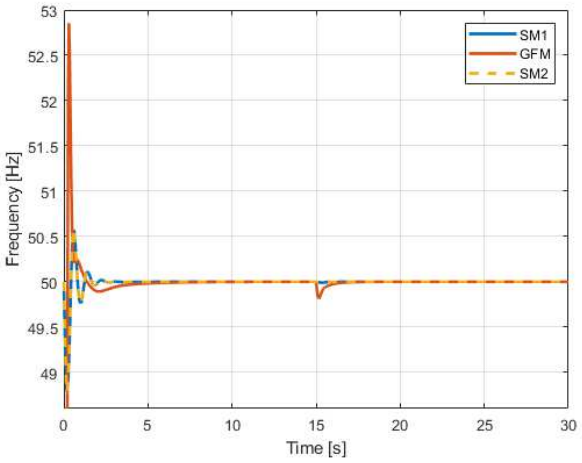

Fig. 5. Frequency of the system consists of 2 SM and a GFM with matching control

TABLE III. FREQUENCY RESPONSE QUANTITIES FOR ALL CONTROL METHODS

		Droop Control			Matching Control			dVOC			SM		
		Settling	Max.	Min.	Settling	Max.	Min.	Settling	Max.	Min.	Settling	Max.	Min.
Initial Response	f [Hz]	49.98	50.38	49.70	49.98	52.86	49.89	50.02	50.04	48.89	50.02	50.58	48.78
	t [s]	4.78	0	2.08	4.77	0.30	2.07	1.56	1.15	0.25	2.310	0.58	0.19
Disturbance at 15 s.	f [Hz]	49.98	50	49.82	49.98	49.99	49.81	49.98	50	49.82	50	50.00	49.99
	t [s]	16.18	15	15.09	16.16	15	15.16	16.19	15	15.09	15	15.00	15.31

TABLE IV. ACTIVE POWER RESPONSE QUANTITIES FOR ALL CONTROL METHODS

		Droop Control			Matching Control			dVOC			SM		
		Settling	Max.	Min.	Settling	Max.	Min.	Settling	Max.	Min.	Settling	Max.	Min.
Initial Response	P [p.u.]	0.77	1.34	0.00	0.77	0.96	-0.16	0.74	3.13	0.68	0.74	1.75	0.00
	t [s]	6.76	2.08	0.00	6.74	2.04	0.35	1.84	0.22	1.13	2.15	0.01	0.00
Disturbance at 15 s.	P [p.u.]	0.77	1.20	0.75	0.77	1.20	0.75	0.77	1.20	0.75	0.75	0.78	0.74
	t [s]	16.76	15.01	15.00	16.74	15.01	15.00	16.78	15.01	15	16.30	15.00	15.01

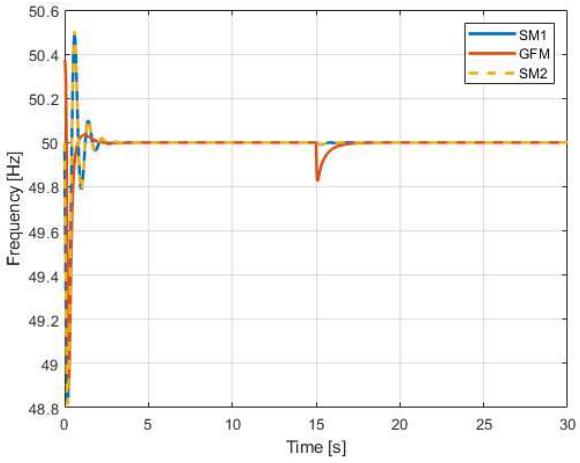

Fig. 6. Frequency of the system consists of 2 SM and a GFM with dVOC

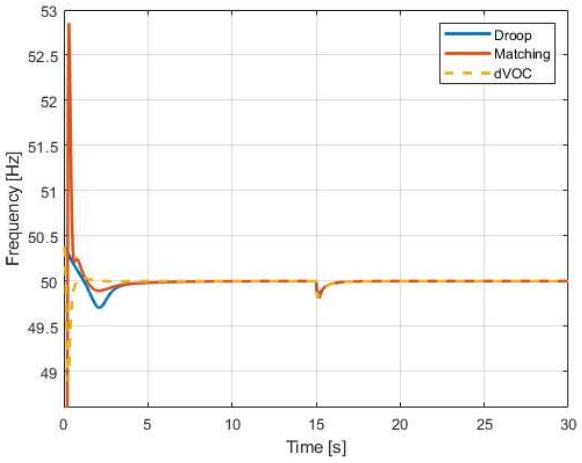

Fig. 7. Comparison of the frequency at the bus to which the GFM converter is connected for all control methods

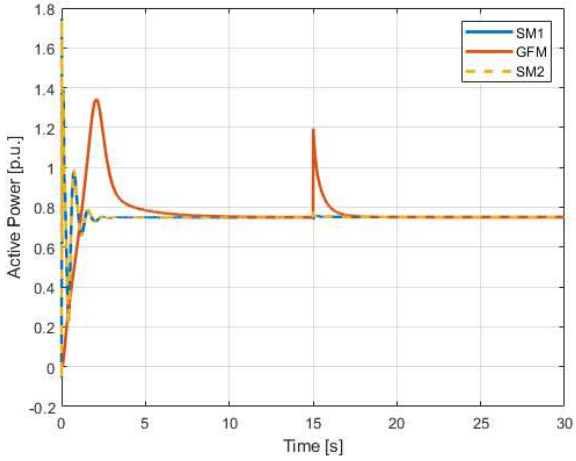

Fig. 8. Active power of the system consists of 2 SM and a GFM with droop control

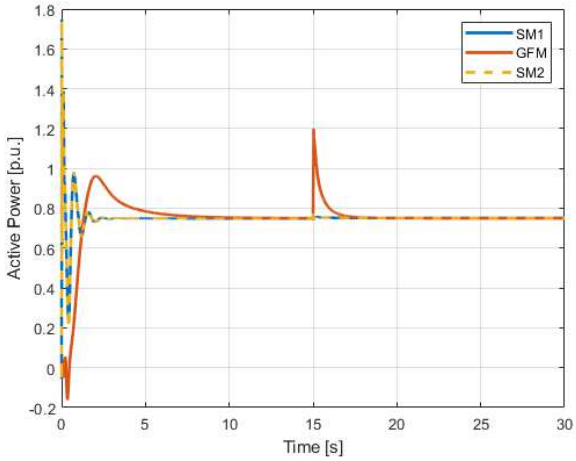

Fig. 9. Active power of the system consists of 2 SM and a GFM with matching control

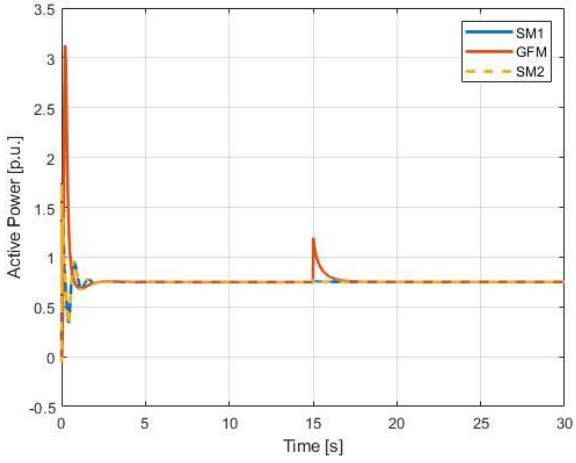

Fig. 10. Active power of the system consists of 2 SM and a GFM with dVOC

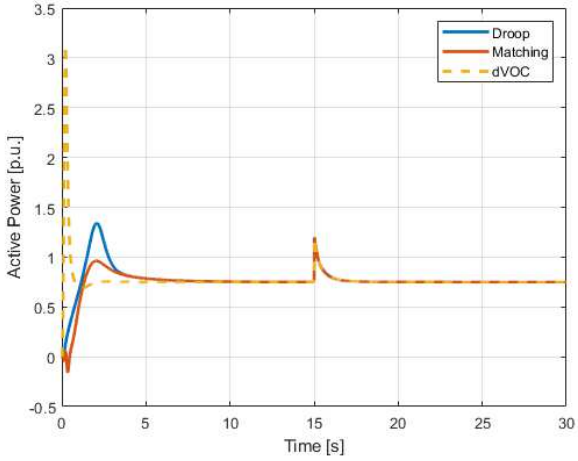

Fig. 11. Comparison of the active power at the bus to which the GFM converter is connected for all control methods

V. Conclusion and Future Work

This study presented a comprehensive analysis of some GFM control techniques on the didactic smart grid system at MCBU-SGlab. Different GFM control techniques such as droop control, matching control and dVOC were applied to the system. Then, frequency and active power at each bus were observed and compared. It was observed that all type of these GFM converters remained stable even severe load disturbance. As a future work, this work could be extended by analyzing the impacts of more GFM techniques and their specialized versions on the system.

References

[1] A. Shrestha and F. Gonzalez-Longatt, "Frequency Stability Issues and Research Opportunities in Converter Dominated Power System," *Energies 2021, Vol. 14, Page 4184*, vol. 14, no. 14, p. 4184, Jul. 2021.

[2] H. Bevrani, H. Golpîra, A. R. Messina, N. Hatziargyriou, F. Milano, and T. Ise, "Power system frequency control: An updated review of current solutions and new challenges," *Electr. Power Syst. Res.*, vol. 194, no. December 2020, 2021.

[3] F. Milano, F. Dorfler, G. Hug, D. J. Hill, and G. Verbič, "Foundations and challenges of low-inertia systems (Invited Paper)," *20th Power Syst. Comput. Conf. PSCC 2018*, Aug. 2018.

[4] R. Rosso, X. Wang, M. Liserre, X. Lu, and S. Engelken, "Grid-Forming Converters: Control Approaches, Grid-Synchronization, and Future Trends—A Review," *IEEE Open J. Ind. Appl.*, vol. 2, pp. 93–109, Apr. 2021.

[5] R. H. Lasseter, Z. Chen, and D. Pattabiraman, "Grid-Forming Inverters: A Critical Asset for the Power Grid," *IEEE J. Emerg. Sel. Top. Power Electron.*, vol. 8, no. 2, pp. 925–935, Jun. 2020.

[6] D. B. Rathnayake *et al.*, "Grid Forming Inverter Modeling, Control, and Applications," *IEEE Access*, vol. 9, pp. 114781–114807, 2021.

[7] J. Matevosyan and J. MacDowell, "ESIG GFM Report," *ESIG GFM Report*, 2022. [Online]. Available: https://www.esig.energy/wp-content/uploads/2022/03/ESIG-GFM-report-2022.pdf. [Accessed: 02-Apr-2022].

[8] A. Tayyebi, D. Grob, A. Anta, F. Kupzog, and F. Dorfler, "Frequency Stability of Synchronous Machines and Grid-Forming Power Converters," *IEEE J. Emerg. Sel. Top. Power Electron.*, vol. 8, no. 2, pp. 1004–1018, Jun. 2020.

[9] J. Matevosyan *et al.*, "Grid-forming inverters: Are they the key for high renewable penetration?," *IEEE Power Energy Mag.*, vol. 17, no. 6, pp. 89–98, Nov. 2019.

[10] W. Du *et al.*, "Modeling of Grid-Forming and Grid-Following Inverters for Dynamic Simulation of Large-Scale Distribution Systems," *IEEE Trans. Power Deliv.*, vol. 36, no. 4, pp. 2035–2045, Aug. 2021.

[11] Y. Khayat *et al.*, "Decentralized optimal frequency control in autonomous microgrids," *IEEE Trans. Power Syst.*, vol. 34, no. 3, pp. 2345–2353, May 2019.

[12] N. Harag, M. Imanaka, M. Kurimoto, S. Shigeyuki, H. Bevrani, and T. Kato, "Autonomous Dual Active Power-Frequency Control in Power System with Small-Scale Photovoltaic Power Generation | SGEPRI Journals & Magazine | IEEE Xplore," 2021. [Online]. Available: https://ieeexplore.ieee.org/abstract/document/9462582. [Accessed: 20-Jan-2022].

[13] J. Liu, Y. Miura, H. Bevrani, and T. Ise, "A Unified Modeling Method of Virtual Synchronous Generator for Multi-Operation-Mode Analyses," *IEEE J. Emerg. Sel. Top. Power Electron.*, vol. 9, no. 2, pp. 2394–2409, Apr. 2021.

[14] A. Singhal, T. L. Vu, and W. Du, "Coordinated Frequency and Voltage Regulation of Grid-Following and Grid-Forming Inverters," *IEEE Trans. Smart Grid*, Dec. 2021.

[15] M. Chen, D. Zhou, A. Tayyebi, E. Prieto-Araujo, F. Dorfler, and F. Blaabjerg, "Generalized Multivariable Grid-Forming Control Design for Power Converters," *IEEE Trans. Smart Grid*, pp. 1–1, Mar. 2022.

[16] M. Chen, D. Zhou, A. Tayyebi, E. Prieto-Araujo, F. Dörfler, and F. Blaabjerg, "Augmentation of Generalized Multivariable Grid-Forming Control for Power Converters with Cascaded Controllers," Feb. 2022.

[17] A. Tayyebi, D. Groß, A. Anta, F. Kupzog, and F. Dörfler, "Interactions of Grid-Forming Power Converters and Synchronous Machines," 2019.

[18] X. Gao, D. Zhou, A. Anvari-Moghaddam, and F. Blaabjerg, "Grid-Following and Grid-Forming Control in Power Electronic Based Power Systems: A Comparative Study," *IECON Proc. (Industrial Electron. Conf.*, vol. 2021-October, Oct. 2021.

[19] H. Zhang, W. Xiang, W. Lin, and J. Wen, "Grid Forming Converters in Renewable Energy Sources Dominated Power Grid: Control Strategy, Stability, Application, and Challenges," *J. Mod. Power Syst. Clean Energy*, vol. 9, no. 6, pp. 1239–1256, Nov. 2021.

[20] M. C. Chandorkar, D. M. Divan, and R. Adapa, "Control of parallel connected inverters in standalone ac supply systems," *IEEE Trans. Ind. Appl.*, vol. 29, no. 1, pp. 136–143, 1993.

[21] C. Arghir, T. Jouini, and F. Dörfler, "Grid-forming control for power converters based on matching of synchronous machines," *Automatica*, vol. 95, pp. 273–282, Sep. 2018.

[22] G. S. Seo, M. Colombino, I. Subotic, B. Johnson, D. Gros, and F. Dorfler, "Dispatchable virtual oscillator control for decentralized inverter-dominated power systems: Analysis and experiments," *Conf. Proc. - IEEE Appl. Power Electron. Conf. Expo. - APEC*, vol. 2019-March, pp. 561–566, May 2019.